Research Article | Vol. 14, No. 5 / 1 May 2024 / Optical Materials Express 1253

Optical Materials EXPRESS

Refractive index measurements of liquids from 0.5 to 2 μm using Rayleigh interferometry

HAO-JUNG CHANG,[1,†] NATALIA MUNERA,[1,†] CESAR LOPEZ-ZELAYA,[1,2] DEBASMITA BANERJEE,[1] GUY BEADIE,[3] ERIC W. VAN STRYLAND,[1] AND DAVID J. HAGAN[1,*]

[1]*CREOL, The College of Optics and Photonics, University of Central Florida, Orlando, Florida 32816, USA*
[2]*Air Force Research Laboratory, Munitions Directorate, Eglin AFB, Florida 32542, USA*
[3]*Peak Nano Optics, LLC, Macedonia, Ohio 44056, USA*
[†]These authors contributed equally to this work
[*]*hagan@creol.ucf.edu*

Abstract: There is growing interest in the refractive index of liquids beyond the visible and into the short-wave infrared (SWIR) for applications such as the study of liquid-core fibers and supercontinuum generation. However, most of the data reported are in the visible. For liquids with a wide transmission window in the SWIR region, refractive index data are sparse. We present a Rayleigh interferometry-based refractometer to characterize the refractive index relative to standard materials at seven different wavelengths (543.4, 632.8, 780, 973, 1064, 1550, and 1970 nm) at a temperature of ~ 21.3 ± 0.6 °C. We also show Sellmeier fits using our results juxtaposed with previously published data. Our data extends previous work to the SWIR.

1. Introduction

The refractive index of liquids has been widely studied in the visible region. Nevertheless, in the SWIR region, there is a lack of data and the dispersion of the refractive index of most liquids is not known. The lack of both is especially true for hydrogen-free solvents, which can exhibit wide transmission windows in the SWIR [1,2]. Some notable examples studied here include carbon tetrachloride, tetrachloroethylene, pentafluorobenzonitrile, bromotrichloromethane, and perfluorohexane. These solvents are good candidates for a variety of recent applications such as in liquid-core optical fibers [3–9], supercontinuum generation [7,10], filamentation [11], nonlinear optics [12], and the design of optofluidic devices [13,14].

Various techniques have been developed to measure the refractive index of liquids. One notable method is Abbe refractometry [15–17], where a liquid is positioned between two prisms, and the refractive index is calculated from Snell's law by measuring the angle at which total internal reflection at the liquid-prism interface occurs. Another technique is minimum deviation [18–22], which involves placing a liquid in a hollow prism and determining its refractive index by minimizing the angle between incident and deflected beams. In a similar method known as beam displacement [23–25], a liquid is contained in a cuvette, and a position-sensitive detector in the far field tracks the movement of the transmitted beam while the cuvette is rotated. With the ellipsometry technique [26,27], the real and imaginary part of the refractive index can be measured by measuring the polarization state change of light at various interfaces, such as air-liquid, prism-liquid, or liquid-solid interfaces. A different approach involves using the Kramers-Kronig relations to calculate the refractive index of a liquid from its absorption spectrum [28]. Finally, there are interferometric techniques, such as Michelson interferometry [29–31] using white light, interference between reflected and transmitted beams from the liquid [32], and interference between a beam passing through the liquid and another passing through a material of known index [33–36].

#519907 https://doi.org/10.1364/OME.519907
Journal © 2024 Received 26 Jan 2024; revised 18 Mar 2024; accepted 25 Mar 2024; published 11 Apr 2024

Optical Materials EXPRESS

We report a technique for measuring the refractive index of liquids by measuring the relative phase between two beams as a function of change in optical path length using a Rayleigh interferometer [37]. Here, the interference is between a beam passing through a sample liquid with unknown refractive index and a beam passing through a reference material with a known refractive index, both beams originating from the same source. We found this technique to be simple to setup, accurate (depending on the choice of reference material and curve fitting), and effective in cases of high loss due to absorption of the sample being measured. We performed this experiment at seven wavelengths (543.4, 632.8, 780, 973, 1064, 1550, and 1970 nm) at a temperature of ~21.3 ± 0.6° C. The dispersion is reported in the form of Sellmeier equations, which are applicable from 543.4 nm to 1970 nm. We include both our experimental results and values reported in the literature spanning the range from 400 nm to 2000 nm.

2. Experiment

The Rayleigh interferometer [37] used in this work is shown in Fig. 1(a). A laser source passes through a half-wave plate (HWP) located between a pair of polarizers (P) to control the power and polarization. The beam then passes through a spatial filter (SF) and is collimated by the first lens (L_b) to form a Gaussian beam (the spatial profile of the 1970 nm case was good enough to not need the spatial filter). This Gaussian beam passes through an opaque plate with two 0.5 mm holes with a center-to-center distance of $h \approx 1.3$ mm to produce two beamlets: the reference beam and the sample beam. For both 1550 nm and 1970 nm, a plate with 0.8 mm holes and $h \approx 2.8$ mm is used. The beamlets are incident on a Starna 63-Q-10 Spectrosil quartz cuvette with two internal chambers of 10 ± 0.01 mm pathlength. One beamlet goes through the sample liquid while the other goes through the reference liquid. In the case of using fused silica as the reference, the Starna 29F-Q-10 cuvette has a single 10 ± 0.01 mm pathlength liquid chamber and the other side is fused silica; essentially mimicking a chamber filled with solid glass. The two spatially and temporally coherent beamlets are then weakly focused by a second lens (L_f) of focal length $f = 1000$ mm for 1064 nm and shorter, and $f = 750$ mm for both 1550 nm and 1970 nm, to create interference fringes. These fringes are measured on one of two cameras, or a detector, depending on the wavelength as described below.

The interference pattern was recorded while the cuvette was rotated to measure the phase difference between the reference and the sample. Since the refractive index of the reference and the sample liquid are different, the two beamlets travel different optical paths as shown in Fig. 1(b). Hence, the relative phase difference between the beamlets can be written as:

$$\Delta\phi(\theta_{in}) = \frac{2\pi L}{\lambda_a}\left[\sqrt{n_{sam}^2 - \sin^2\theta_{in}} - \sqrt{n_{ref}^2 - \sin^2\theta_{in}}\right] - \Delta\phi_0, \tag{1}$$

where θ_{in} is the angle of incidence, λ_a is the wavelength in air, n_{sam} and n_{ref} are the sample and reference relative refractive indices, respectively, and $\Delta\phi_0 = \frac{2\pi L}{\lambda_a}\left[n_{sam} - n_{ref}\right]$ is included to ensure that $\Delta\phi(0°) = 0$. The relative refractive index is defined as a material's absolute refractive index divided by the refractive index of the surrounding air. We follow the standard practice used in optical glass catalogs and provide dispersion data in the form of relative refractive index values. Unless otherwise stated, all results and tabulated coefficients refer to the presentation of relative refractive index values as a function of wavelengths in air.

As the cuvette is rotated, the beamlets undergo different displacements due to refraction. These vertical displacements, $\delta Y_{sam}(\theta_{in})$ and $\delta Y_{ref}(\theta_{in})$, result in an additional pathlength, $\delta P(\theta_{in})$, as shown in Fig. 1(b) – the additional pathlength, $\delta P(\theta_{in})$, is accounted for in Eq. (1). The expressions for $\delta Y_{sam}(\theta_{in})$ and $\delta Y_{ref}(\theta_{in})$ were derived in [23] and are given by: $\delta Y_{sam}(\theta_{in}) = \left[2L_g\left(1 - \frac{\cos\theta_{in}}{\sqrt{n_g^2 - \sin^2\theta_{in}}}\right) + L\left(1 - \frac{\cos\theta_{in}}{\sqrt{n_{sam}^2 - \sin^2\theta_{in}}}\right)\right]\sin\theta_{in}$, where $L_g = 1.25$ mm is the thickness of

Optical Materials EXPRESS

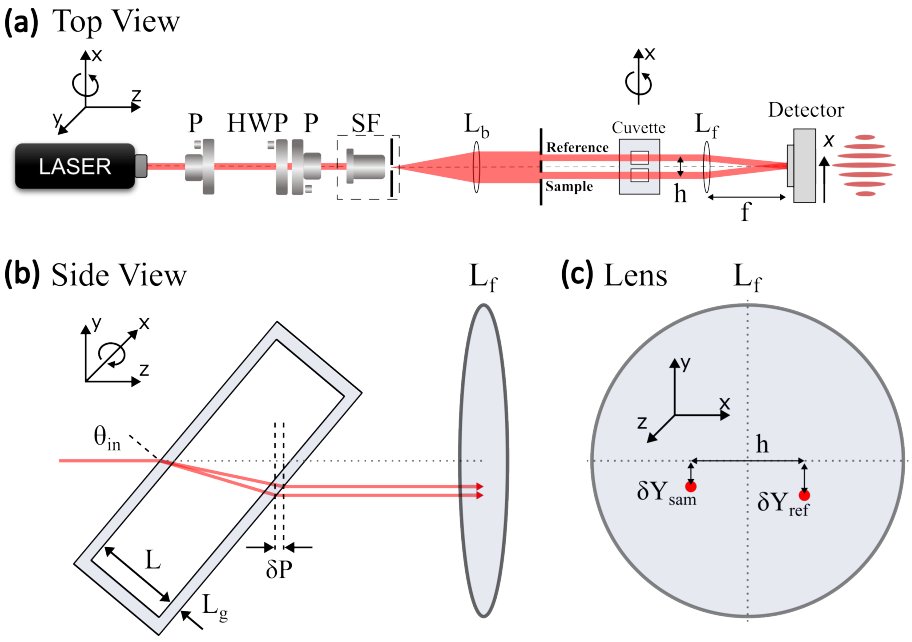

Fig. 1. (a) Top view of the optical setup. (b) Side view showing how rotating the cuvette about the x-axis changes the incident angle, θ_{in}. The beamlets refract at different angles and experience different optical paths due to the refractive indices of the sample, n_{sam}, and reference, n_{ref}. (c) Consequently, the beamlets become vertically misaligned on the second lens, L_f, by δY_{sam} and δY_{ref}.

the cuvette walls, and n_g is the refractive index of Spectrosil quartz at a specific wavelength; a similar expression where n_{ref} is used instead corresponds to $\delta Y_{ref}(\theta_{in})$.

In Fig. 1(b) and (c), the beam separations are greatly exaggerated to show the pathlength differences. In actuality, for a maximum incident angle, $\theta_{in} = 20°$, $n_{sam} > n_{ref}$ and $n_{sam} - n_{ref} \leq 0.1$, the maximum change in the angle between the two beamlets within the cuvette is $\sim 1°$. Consequently, the difference in the vertical displacement of the two beamlets is $\Delta Y(20°) = \delta Y_{sam}(20°) - \delta Y_{ref}(20°) < 200$ µm, as shown greatly exaggerated in Fig. 1(b) and (c). The difference in the vertical displacement can lead to a slight xy-plane tilt of the fringes by an angle $\theta_{tilt} = \tan^{-1}(\Delta Y(20°)/h)$. This causes the spacing of the fringes to be slightly modified; however, along the x direction, which is what is measured, the observed spacing is unchanged. Additionally, for the lens effective $f\# = h/f$ used in this work, $\sim f/769$ for the visible (up to 1064 nm) and $\sim f/268$ for the SWIR (1550 nm and 1970 nm), we can safely ignore aberrations.

The phase difference, $\Delta\phi$, changes with incident angle, causing the interference fringes to move. To verify this, we used identical index matching liquids on the cuvette, which caused the interference pattern to stay constant in response to the cuvette rotation. This proved to us that the relative phase was unchanged. Figure 2 shows the interferogram between a cyclohexane sample (which is unknown in our case) and Fused Silica Matching Liquid Code 50350 (see Dataset 1 [38]) as the known reference. Figure 2(a) shows the cross-section of the interference fringes as a function of position on the camera for several different incident angles. We set the average distance between fringe maxima to be a phase change of 2π, and the positions of the maxima (red markers) as a function of incident angle are shown in Fig. 2(b). The unknown refractive index of the sample liquid, n_{sam}, is then obtained by fitting Eq. (1) (solid black lines) to the experimental data, where the adjustable parameters are n_{sam} and the distance between interference maxima.

Optical Materials EXPRESS

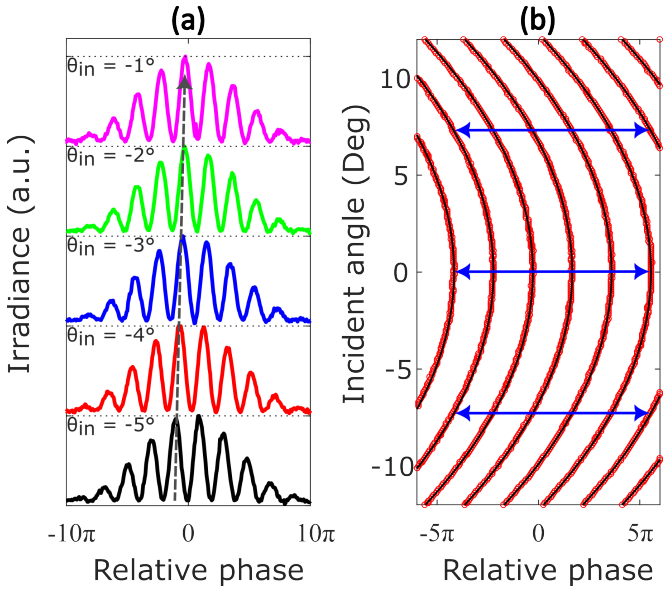

Fig. 2. (a) Cross-section of the interference fringes at five different incident angles for cyclohexane using fused silica index matching liquid as a reference at 543.4 nm. Gray dashed arrow represents fringe displacement. (b) Interference maxima plotted vs. incident angle from camera image (red markers) along with fits to Eq. (1) (solid black lines). Blue horizontal arrows of equal length represent a 10π relative phase.

Seven laser sources were used: two helium-neon lasers with central wavelengths at 543.4 nm (Melles Griot, 05-LGR-025-S) and 632.8 nm (Melles Griot, 05-LHP-171), two diode lasers with central wavelengths at 780 nm and 973 nm (the wavelength was measured with an Ocean Optics spectrometer), a microchip laser (Teem Photonics, MLC-0240DR1) at 1064 nm, a laser diode module (Thorlabs, LDM1550) at 1550 nm and a thulium fiber laser (AdValue, AP-QS-MOD) at 1970 nm. The reference materials are the 29F-Q-10 cuvette wall (Spectrosil quartz from Heraeus) and refractive index liquids from Cargille labs loaded on the side channel of the 63-Q-10 cuvette. Cargille labs provided the refractive indices of the reference liquids relative to vacuum. To convert these to values relative to air, we multiplied them by $1/n_{\text{air}}$. In contrast, the refractive indices for the Spectrosil quartz reference were already given relative to air by Heraeus. For more information on what reference material was used for each liquid at each wavelength, see Dataset 1 [38]. The detectors are a silicon beam profiler (Coherent, LASERCAM HR) for the shortest five wavelengths, an InGaAs camera (Sensors Unlimited, SU640CSX) for 1550 nm, and a 20 μm pinhole attached to a PbSe detector (Thorlabs, PDA20H) for 1970 nm. The silicon beam profiler was used to generate the full fringe trajectory pattern shown in Fig. 2(b). This pattern was generated through repeated scans at various incident angles, a process that only required a few minutes. Similarly, employing the InGaAs camera at 1550 nm to generate equivalent patterns also took only a few minutes. In contrast, scans with the PbSe detector at 1970 nm took ~12 hours. For instance, when examining trichloroacetonitrile at 1970 nm, the interference fringes were scanned across 161 detector positions for each of the 151 incident angles. For the angular rotations, a Newport universal motion controller driver model ESP300 was used to rotate a Micro-Controle Spectra-Physics rotation stage. The temperature is measured by an external thermometer (Xsensior). All measurements are done at ~ 21.3 ± 0.6° C. All the solvents are commercially available as referenced in Tables 1–5, and used without further purification.

Optical Materials EXPRESS

Table 1. Relative refractive index of benzene derivatives in this work and literature

Liquid and Temp.	Wavelength (nm)	This work	Literature
Benzene C_6H_6 Sigma-Aldrich T = 21.5 ± 0.4° C	543.4	1.5037(5)	1.4999(27) [39], 1.5055(20) [33], 1.5056(20) [40]*
	632.8	1.4964(5)	1.4925(27) [39]*, 1.495137(25) [36]*, 1.497866(20) [33]* 1.4980(20) [40]
	780	1.4888(2)	1.4859(27) [39], 1.4908(20) [40]
	973	1.4843(10)	1.4815(27) [39], 1.4857(20) [40]
	1064	1.4842(10)	1.4802(27) [39], 1.4814(25,1) [25]*, 1.4808(25,5) [25]*, 1.4841(20) [40]
	1550	1.4797(3)	1.4769(27) [39]*, 1.4789(25,3) [17], 1.4767(27) [28]*, 1.4777(27) [28]**, 1.4799(20) [40]
	1970	1.4780(6)	1.4774(27) [28]**, 1.4784(20) [40]
Toluene $C_6H_5CH_3$ ACROS T = 21.9 ± 0.8° C	543.4	1.4993(5)	1.4961(27) [39], 1.5009(20) [16], 1.4979(20) [34], 1.5009(20) [40], 1.4996(22) [41]
	632.8	1.4914(6)	1.4890(27) [39]*, 1.4936(20) [16], 1.491218(25) [36]*, 1.495612(20) [34]*, 1.4936(20) [40], 1.4940(22) [41]
	780	1.4850(2)	1.4824(27) [39], 1.4870(20) [16], 1.4869(20) [40]
	973	1.4805(10)	1.4781(27) [39], 1.4825(20) [16], 1.4824(20) [40]
	1064	1.4800(10)	1.4769(27) [39], 1.4812(20) [16], 1.4784(25,1) [25]*, 1.4777(25,3) [25]*, 1.4811(20) [40]
	1550	1.4768(4)	1.4737(27) [39]* , 1.4778(20) [16], 1.4760(25,2) [17], 1.4735(27) [28]*, 1.4741(27) [28]**, 1.4777(20) [40]
	1970	1.4753(4)	1.4744(27) [28]**, 1.4764(20) [40]
P-Xylene $C_6H_4(CH_3)_2$ Sigma-Aldrich T = 21.8 ± 0.5° C	543.4	1.4976(2)	
	632.8	1.4915(5)	
	780	1.4867(4)	
	973	1.4786(10)	
	1064	1.4800(10)	
	1550	1.4759(3)	1.4753(25,1) [17]
	1970	1.4751(4)	
Pyridine C_6H_5N Sigma-Aldrich T = 21.7 ± 0.5° C	543.4	1.5115(6)	
	632.8	1.5038(6)	
	780	1.4978(3)	
	973	1.4938(10)	
	1064	1.4923(10)	
	1550	1.4880(3)	1.4851(27) [28]*, 1.4857(27) [28]**
	1970	1.4864(7)	
Nitrobenzene $C_6H_5NO_2$ Sigma-Aldrich T = 21.9 ± 0.8° C	543.4	1.5567(6)	
	632.8	1.5462(7)	
	780	1.5353(5)	
	973	-	
	1064	1.5264(10)	1.5262(25,2) [25]*
	1550	1.5223(5)	
	1970	1.5199(7)	1.5212(27) [28]**

Optical Materials EXPRESS

Table 2. Relative refractive index of haloalkanes in this work and literature

Liquid and Temp.	Wavelength(nm)	This work	Literature
Dichloromethane CH_2Cl_2 Merck KGaA T = 21.6 ± 0.5° C	543.4	1.4258(5)	
	632.8	1.4217(3)	
	780	1.4180(4)	
	973	-	
	1064	1.4150(10)	1.4120(6) [25]*
	1550	1.4133(2)	1.4124(25,2) [17], 1.4125(25) [42]
	1970	1.4126(4)	1.4121(25) [42]
Chloroform $CHCl_3$ Sigma-Aldrich T = 21.6 ± 0.8° C	543.4	1.4472(2)	1.4464(20) [16], 1.4520(20) [34], 1.4485(20) [40]
	632.8	1.4436(5)	1.3323(20) [16], 1.441415(20) [34]*, 1.4443(20) [40]
	780	1.4380(4)	1.4385(20) [16], 1.4401(20) [40]
	973	1.4370(10)	1.4361(20) [16], 1.4371(20) [40]
	1064	1.4347(10)	1.4354(20) [16], 1.4331(25,4) [25]*, 1.4362(20) [40]
	1550	1.4332(10)	1.4334(20) [16], 1.4321(25,1) [17], 1.4337(20) [40]
	1970	1.4315(3)	1.4326(20) [40]
Carbon tetrachloride CCl_4 Sigma-Aldrich T = 22.0 ± 0.9° C	543.4	1.4599(4)	1.4593(27) [39], 1.4621(20) [16]
	632.8	1.4566(4)	1.4551(27) [39]*, 1.4579(20) [16], 1.455852(25) [36]*
	780	1.4522(5)	1.4513(27) [39] , 1.4539(20) [16]
	973	1.4510(10)	1.4488(27) [39], 1.4521(20) [16]
	1064	1.4498(10)	1.4481(27, 1) [39], 1.4504(20) [16], 1.4477(25,2) [25]*, 1.4557(25) [43]
	1550	1.4468(3)	1.4464(27) [39]*, 1.4483(20) [16], 1.4530(25) [43]
	1970	1.4457(2)	1.4530(25) [43]

Optical Materials EXPRESS

Table 3. Relative refractive index of alcohols in this work and literature

Liquid and Temp.	Wavelength(nm)	This work	Literature
Methanol CH_3OH ACROS T = 21.5 ± 0.3° C	543.4	1.3292(4)	1.3284(27) [39], 1.3376(20) [33], 1.3295(22) [41]
	632.8	1.3270(5)	1.3259(27) [39]*, 1.326343(20) [33]*, 1.3270(22) [41]
	780	1.3224(5)	1.3234(27) [39]
	973	1.3210(10)	1.3215(27) [39]
	1064	1.3190(10)	1.3207(27) [39], 1.3198(25,3) [25]*
	1550	-	1.3172(27) [39]*, 1.3174(25,1) [17], 1.4201(26) [28]*, 1.3115(26) [28]**
	1970	1.3164(8)	1.3074(26) [28]**
Ethanol C_2H_5OH Sigma-Aldrich T = 21.6 ± 0.6° C	543.4	1.3627(3)	1.3631(20) [16], 1.3626(22) [41]
	632.8	1.3604(3)	1.3603(20) [16], 1.358853(25) [36]*, 1.3593(22) [41]
	780	1.3580(6)	1.3575(20) [16]
	973	1.3543(10)	1.3554(20) [16]
	1064	1.3548(10)	1.3547(20) [16]
	1550	1.3523(10)	1.3520(20) [16], 1.3503(25,3) [17], 1.3495(26) [28]*, 1.3474(26) [28]**
	1970	1.3482(6)	1.3447(26) [28]**
1-propanol C_3H_8O Sigma-Aldrich T = 21.7 ± 0.7° C	543.4	1.3863(3)	1.3846(27) [39]
	632.8	1.3828(4)	1.3941(27) [39]*, 1.397105(20) [33]*
	780	1.3810(5)	1.3913(27) [39]
	973	1.3783(10)	1.3890(27) [39]
	1064	1.3783(10)	1.3883(27) [39]
	1550	1.3751(10)	1.3858(27) [39]*
	1970	1.3725(4)	
1-butanol $C_4H_{10}O$ Sigma-Aldrich T = 21.6 ± 0.6° C	543.4	1.3999(2)	1.3970(27) [39]
	632.8	1.3978(2)	1.3941(27) [39]*, 1.397105(20) [33]*
	780	1.3950(4)	1.3913(27) [39]
	973	1.3922(10)	1.3890(27) [39]
	1064	1.3916(10)	1.3883(27) [39]
	1550	1.3890(10)	1.3858(27) [39]*
	1970	1.3868(6)	
1-octanol $C_8H_{18}O$ Sigma-Aldrich T = 21.7 ± 0.6° C	543.4	1.4305(2)	
	632.8	1.4273(2)	
	780	1.4235(4)	
	973	1.4226(10)	
	1064	1.4210(10)	
	1550	1.4190(10)	
	1970	1.4163(2)	

Optical Materials EXPRESS

Table 4. Relative refractive index of SWIR transparent solvents

Liquid and Temp.	Wavelength(nm)	This work	Literature
Carbon disulfide CS_2 Sigma-Aldrich T = 21.7 ± 0.8° C	543.4	1.6319(9)	1.6373(20) [9], 1.6361(20) [16], 1.6367(20) [40]
	632.8	1.6177(10)	1.6213(20) [9], 1.6211(20) [16], 1.617672(25) [36]*, 1.623977(20) [34]*, 1.6212(20) [40]
	780	1.6019(11)	1.6066(20) [9], 1.6072(20) [16], 1.6069(20) [40]
	973	-	1.5968(20) [9], 1.5981(20) [16], 1.5974(20) [40]
	1064	1.5950(10)	1.5939(20) [9], 1.5955(20) [16], 1.5910(25,3) [25]*, 1.5946(20) [40]
	1550	1.5834(7)	1.5857(20) [9], 1.5885(20) [16], 1.5872(20) [40]
	1970	1.5802(10)	1.5812(20) [9], 1.5843(20) [40]
Pentafluorobenzonitrile C_6F_5CN Sigma-Aldrich T = 21.6 ± 0.5° C	543.4	1.4453(5)	
	632.8	1.4381(2)	
	780	1.4332(3)	
	973	1.4295(10)	
	1064	1.4240(10)	1.4254(25,4) [25]*
	1550	1.4241(4)	
	1970	1.4213(4)	
Bromotrichloromethane $BrCCl_3$ Sigma-Aldrich T = 21.6 ± 0.5	543.4	1.5080(6)	
	632.8	1.5016(5)	
	780	1.4958(2)	
	973	-	
	1064	1.4932(10)	
	1550	1.4895(3)	
	1970	1.4881(6)	
Perfluorohexane C_6F_{14} Alfa Aesar T = 21.5 ± 0.3	543.4	1.2524(4)	
	632.8	1.2509(4)	
	780	1.2495(6)	
	973	1.2480(10)	
	1064	1.2480(10)	
	1550	1.2475(10)	
	1970	1.2462(13)	
Tetrachloroethylene C_2Cl_4 Sigma-Aldrich T = 21.7 ± 0.6° C	543.4	1.5068(6)	
	632.8	1.5015(3)	
	780	1.4955(3)	
	973	1.4917(10)	
	1064	1.4907(10)	
	1550	1.4879(4)	
	1970	1.4864(5)	
Trichloroacetonitrile C_2Cl_3N Sigma-Aldrich T = 21.5 ± 0.5° C	543.4	1.4382(4)	
	632.8	1.4348(6)	
	780	1.4318(6)	
	973	-	
	1064	1.4280(10)	
	1550	1.4258(9)	
	1970	1.4265(8)	
Trifluoroacetic anhydride $C_4F_6O_3$ Sigma-Aldrich T = 21.1 ± 0.7° C	543.4	1.2708(5)	
	632.8	1.2685(3)	
	780	1.2661(5)	
	973	-	
	1064	1.2645(10)	
	1550	1.2641(9)	
	1970	1.2628(11)	

Optical Materials EXPRESS

Table 5. Relative refractive index of other common solvents

Liquid and Temp.	Wavelength(nm)	This work	Literature
Acetone C_3H_6O Sigma-Aldrich T = 21.5 ± 0.2° C	543.4	1.3590(5)	
	632.8	1.3568(4)	
	780	1.3525(5)	
	973	1.3520(10)	
	1064	1.3490(10)	1.3487(25,4) [25]*
	1550	1.3487(10)	1.3483(25,2) [17]
	1970	1.3477(6)	
Acetonitrile C_2H_3N Sigma-Aldrich T = 21.4 ± 0.3° C	543.4	1.3440(3)	1.3418(27) [39], 1.3438(22) [41]
	632.8	1.3416(6)	1.3393(27) [39]*, 1.3408(22) [41]
	780	1.3395(5)	1.3373(27) [39]
	973	1.3365(10)	1.3361(27) [39]
	1064	1.3357(10)	1.3357(27) [39], 1.3354(25,3) [25]*
	1550	1.3358(10)	1.3345(27) [39]*, 1.3335(26) [28]*, 1.3337(26) [28]**, 1.3348(25,2) [17]
	1970	1.3339(7)	1.3335(26) [28]**
Hexane C_6H_{14} Sigma-Aldrich T = 21.5 ± 0.5° C	543.4	1.3770(4)	1.3776(22) [41]
	632.8	1.3736(3)	1.3743(22) [41]
	780	1.3712(5)	
	973	1.3688(10)	
	1064	1.3698(10)	
	1550	1.3670(10)	
	1970	1.3668(3)	
Cyclohexane C_6H_{12} ACROS T = 21.5 ± 0.6° C	543.4	1.4268(3)	1.4273(22) [41]
	632.8	1.4242(2)	1.4238(22) [41]
	780	1.4215(4)	
	973	1.4185(10)	
	1064	1.4180(10)	1.4158(25,4) [25]*
	1550	1.4158(3)	1.4147(25,11) [17]
	1970	1.4147(4)	
Tetrahydrofuran C_4H_8O ACROS T = 21.6 ± 0.7° C	543.4	1.4084(2)	
	632.8	1.4053(2)	
	780	1.4025(3)	
	973	1.4008(10)	
	1064	1.4000(10)	1.3974(25,1) [25]*
	1550	1.3983(10)	1.3969(25,3) [17]
	1970	1.3961(4)	
1,4-Dioxane $C_4H_8O_2$ Sigma-Aldrich T = 21.6 ± 0.5° C	543.4	1.4241(3)	1.4219(27) [39]
	632.8	1.4197(5)	1.4190(27) [39]*
	780	1.4179(3)	1.4165(27) [39]
	973	1.4148(10)	1.4148(27) [39]
	1064	1.4150(10)	1.4143(27) [39], 1.4119(25,2) [25]*
	1550	1.4123(10)	1.4124(27) [39]*, 1.4127(25, 5) [17]
	1970	1.4108(4)	

Optical Materials EXPRESS

3. Results

The experimental results are presented in Tables 1–5 along with literature data. The first column lists the sample liquids being characterized, their chemical formula, the vendors we obtained them from, and the average temperature at which the measurements were done. In the third column, parentheses indicate the total uncertainty (±) in the 4th decimal place, while the fourth column's parentheses denote both the measurement temperature and the measurement uncertainty (±) in the 4th decimal place, respectively. A star (*) in the literature column indicates that the value is calculated from the dispersion function reported in the corresponding literature. Double stars (**) in Ref. [28] indicate values calculated from Kramers-Kronig relations. The reference refractive index for each sample was typically chosen to yield an index difference, $|n_{sam} - n_{ref}|$, between ~0.01 and 0.1 to accurately fit Eq. (1) to the experimental data, such as in Fig. 2(b). Dataset 1 [38] contains the % transmittance spectrum for each sample measured with a Cary 5000 spectrophotometer from 400 to 2000 nm. The transmittance spectrum for each sample includes the reflection loss from the 10 mm pathlength Spectrosil quartz cuvette. The absorption of the cuvette in this wavelength region is negligible. Dataset 1 [38] also includes the reference refractive index liquids used at each wavelength and the experimental results measured in this work.

The primary contributors to the uncertainty in the measured refractive indices include the uncertainty in the index of the reference material, as provided by the manufacturer (see Dataset 1 [38]), and the fitting uncertainties. To determine the fitting error, we identified the value of n_{sam} and we set the phase between fringes to be 2π. We then adjusted n_{sam} by an offset $\pm\Delta$ that fit the experimental data adequately. The range between the highest and lowest refractive indices that still produced adequate fits of the data determines Δn_{sam}, i.e., the fitting uncertainties. For most liquids, the fitting error was $\Delta n_{sam} \lessapprox 3 \cdot 10^{-4}$. Two of the authors independently fit several of the indices for different materials as well as a couple of different wavelengths, and the results always agreed to within ±0.0002. The total uncertainties including the reference etc. are in Tables 1–5 but in general are $\lessapprox 10 \cdot 10^{-4}$, while perfluorohexane and trifluoroacetic anhydride, the liquids with the lowest refractive indices, exhibited maximum fitting uncertainties in the order of $\sim 13 \cdot 10^{-4}$. Ultimately, the total uncertainties can be reduced, i.e., the technique's accuracy can be increased, by choosing well-calibrated reference materials with lower uncertainty in their refractive index and with improved curve-fitting algorithms.

We also considered uncertainties due to temperature, geometrical tolerances of the cuvette, and laser wavelength. However, these uncertainties were smaller than the primary contributors discussed above. Temperatures in the laboratory fluctuated by ~1% resulting in uncertainties beyond the resolution limit set forth by the experiment. The cuvette pathlength is known to an accuracy of 0.1% (from the manufacturer, Starna), however knowing the accuracy is redundant due to both the sample and reference liquids being in the same cuvette. For the contribution of the wavelength uncertainty to remain below the $2 \cdot 10^{-4}$ threshold, which is the lowest total uncertainty reported in Tables 1–5, the maximum tolerable uncertainty for the wavelengths we used 543.4, 632.8, 780, 973, 1064, 1550, and 1970 nm is ± 0.5, 0.8, 1.6, 3.0, 3.8, 8.4, and 9.2 nm, respectively. We do not need to know the absolute angle since $\Delta\phi(0°)$ is the origin of Eq. (1) centered at 0°. However, we do need to know the relative angle change accurately to fit Eq. (1) to the experimental data. The experimental accuracy to which we know the angle is 0.01°; this level of accuracy translates to an uncertainty in refractive index of <0.0001.

Despite the high loss due to absorption of some liquids at specific wavelengths, such as 1550 nm for the alcohols, the refractive index could still be measured with a fringe peak-to-minimum contrast as low as 0.7% – corresponding to ethanol. Ideally, from the equation of interference of two beams (assuming monochromatic plane-waves), we expect a ~20% fringe contrast for ~1% transmission through the liquid. Methanol, on the other hand, exhibits higher absorption at 1550 nm, and thus the fringe contrast was beyond what the InGaAs camera could resolve.

Optical Materials EXPRESS

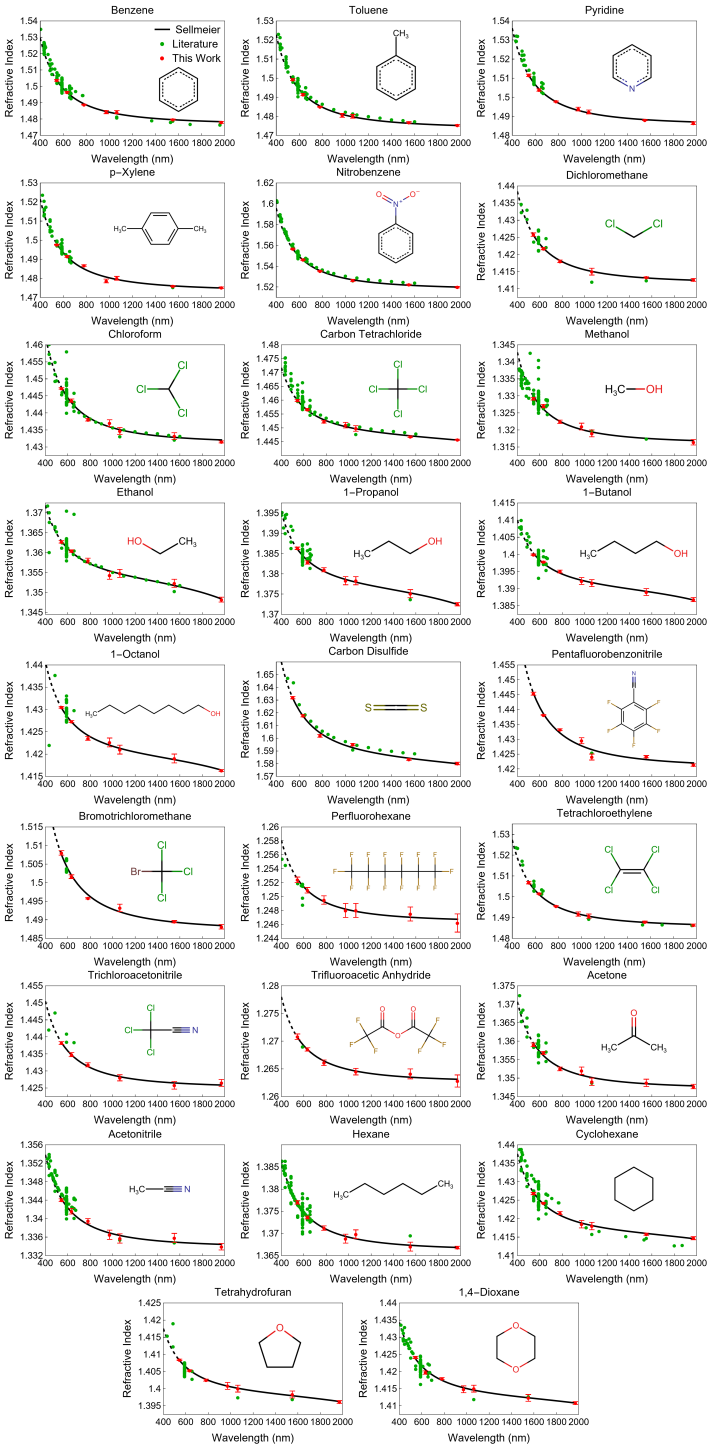

Fig. 3. Sellmeier fits of the relative refractive index data reported in this work along with literature data. Solid and dashed portions show fits to results measured in this work and their extrapolation, respectively. The temperatures associated with each solid curve are specified in Tables 1–5, ranging from 21.1 ° C to 22.0 ° C.

Optical Materials EXPRESS

Table 6. Sellmeier coefficients for fits to the relative refractive index of different solvents. Wavelengths are expressed in nm, and the temperatures at which the data for these curves were measured are specified in Tables 1–5, ranging from 21.1 ° C to 22.0 ° C.

Solvent	B_{UV}	λ_{UV}	B_{IR}	λ_{IR}
Benzene	1.180	138	0	-
Toluene	1.171	134	0	-
p-Xylene	1.170	133	0	-
Pyridine	1.206	135	0	-
Nitrobenzene	1.302	159	0	-
Dichloromethane	0.9923	107	0	-
Chloroform	1.047	114	0	-
Carbon tetrachloride	1.094	99.6	0.290	12900
Methanol	0.7316	119	0	-
Ethanol	0.8312	96.4	0.0192	2970
1-Propanol	0.8940	94.4	0.0158	2970
1-Butanol	0.9314	95.9	0.0137	2970
1-Octanol	1.013	96.5	0.0112	2900
Carbon disulfide	1.502	169	0.163	6520
Pentafluorobenzonitrile	1.017	140	0	-
Bromotrichloromethane	1.211	120	0	-
Perflourohexane	0.5532	90.1	0	-
Tetrachloroethylene	1.206	124	0	-
Trichloroacetonitrile	1.030	103	0	-
Trifluoroacetic Anhydride	0.5939	99.7	0	-
Acetone	0.8144	108	0	-
Acetonitrile	0.7786	102	0	-
Hexane	0.8660	98.8	0	-
Cyclohexane	1.004	97.1	0.0108	3450
Tetrahydrofuran	0.9544	93.5	0.0147	3450
1,4-Dioxane	0.9937	98.2	0.0121	3450

In principle, a neutral density filter could be introduced in the reference arm to increase the contrast; however, this was not needed to keep our uncertainties lower than the uncertainties in our reference materials. We did not attempt this due to the added complexity. With acetonitrile, one of the materials that exhibits high loss, we performed experiments at three different power levels (25%, 50%, and 75% of max) at 1970 nm and did not observe any difference in the measured index values that could arise from heating and thermal expansion, i.e., from the thermo-optic effect [44].

Dispersion relations are obtained by fitting the Sellmeier equation:

$$n^2 - 1 = \frac{B_{UV}\lambda^2}{\lambda^2 - \lambda_{UV}^2} + \frac{B_{IR}\lambda^2}{\lambda^2 - \lambda_{IR}^2} \tag{2}$$

to the measured relative refractive index values. In Eq. (2), B_{UV} and B_{IR} are Sellmeier coefficients and λ_{UV} and λ_{IR} are resonances in the UV and IR, respectively. Fits were obtained by using Wolfram Mathematica's "NonlinearModelFit" command with the Levenberg–Marquardt method. The fitting algorithm automatically solved for B_{UV}, B_{IR}, and λ_{UV} resonances, while λ_{IR} resonances

Optical Materials EXPRESS

were manually set to the strongest molecular vibration beyond 1970 nm obtained from NIST [45] and AIST [46]. Although some of the liquids exhibit absorption bands in the SWIR ($\gtrsim$ 1000 nm), their refractive indices were fit using a single UV Sellmeier term (e.g., acetone). On the other hand, for other liquids the inclusion of an IR term was necessary to enhance fitting accuracy at longer wavelengths (e.g., most alcohols). Table 6 shows the Sellmeier coefficients and resonances, in nanometers (nm), obtained by only fitting the data we measured. Note that we extended these Sellmeier fits from 543.4 nm down to 400 nm with dotted lines for comparison with literature experimental values; the uncertainty of results extrapolated down to 400 nm is ~5 to 6 times greater than the uncertainty of the measured data. In Fig. 3 we compare our Sellmeier fits and measured indices with data from Landolt–Börnstein [47] and from the broader literature (see Tables 1–5 and the cited publications, excluding the starred values). We focus on literature data at wavelengths from 400 nm to 2000 nm, and temperatures from 15° C to 25° C.

4. Conclusion

We developed a simple experimental technique to measure the refractive index of liquids relative known materials. This Rayleigh interferometer-based refractometer measures the refractive index by tracking the movement of the peaks of interference fringes the angle of incidence is varied. It is simple to set up, accurate (depending on the choice of reference material and curve fitting), and can effectively measure samples even in cases of relatively high absorption. This study presented the refractive index measurement of 26 solvents at 7 different wavelengths (543.4, 632.8, 780, 973, 1064, 1550, and 1970 nm) and includes data from the literature. Thus, it extended the wavelength range deeper into the SWIR for most of these materials where data were not present. We also report the dispersion relationships for all the solvents using fitted Sellmeier equations to the above wavelengths extended to the range from 400 nm to 2 μm juxtaposed with available reference data taken between 15° C to 25° C.

Funding. Air Force Research Laboratory (FA86511820019).

Acknowledgments. We thank Scott Webster for fabricating the pinholes for producing the two beamlets, we thank Robert Norwood and Seth Marder for suggesting SWIR transparent liquids to characterize, and we thank Christian Keyser for introducing to us the lack of refractive index data in the IR, lending us the 1970 nm thulium fiber laser laser, and for stimulating discussions. We also thank Markus Schmidt (private communication) for reports of a better fit to his liquid-filled fiber nonlinearities using our data for carbon tetrachloride.

Disclosures. The authors declare no conflicts of interest.

Data availability. Data underlying the results presented in this paper are available in Dataset 1, Ref. [38].

References

1. J. Campo, F. Desmet, W. Wenseleers, *et al.*, "Highly sensitive setup for tunable wavelength hyper-Rayleigh scattering with parallel detection and calibration data for various solvents," Opt. Express **17**(6), 4587–4604 (2009).
2. S. Junaid, W. Huang, R. Scheibinger, *et al.*, "Attenuation coefficients of selected organic and inorganic solvents in the mid-infrared spectral domain," Opt. Mater. Express **12**(4), 1754–1763 (2022).
3. F. M. Cox, A. Argyros, and M. C. J. Large, "Liquid-filled hollow core microstructured polymer optical fiber," Opt. Express **14**(9), 4135–4140 (2006).
4. Y. Zhu, X. Chen, Y. Xu, *et al.*, "Propagation properties of single-mode liquid-core optical fibers with subwavelength diameter," J. Lightwave Technol. **25**(10), 3051–3056 (2007).
5. R. Zhang, J. Teipel, X. Zhang, *et al.*, "Group velocity dispersion of tapered fibers immersed in different liquids," Opt. Express **12**(8), 1700–1707 (2004).
6. M. Vieweg, T. Gissibl, S. Pricking, *et al.*, "Ultrafast nonlinear optofluidics in selectively liquid-filled photonic crystal fibers," Opt. Express **18**(24), 25232–25240 (2010).
7. J. Bethge, A. Husakou, F. Mitschke, *et al.*, "Two-octave supercontinuum generation in a water-filled photonic crystal fiber," Opt. Express **18**(6), 6230–6240 (2010).
8. K. Kieu, L. Schneebeli, R. A. Norwood, *et al.*, "Integrated liquid-core optical fibers for ultra-efficient nonlinear liquid photonics," Opt. Express **20**(7), 8148–8154 (2012).
9. M. Chemnitz, M. Gebhardt, C. Gaida, *et al.*, "Hybrid soliton dynamics in liquid-core fibres," Nat. Commun. **8**(1), 42 (2017).

Optical Materials EXPRESS

10. J. Liu, H. Schroeder, S. L. Chin, *et al.*, "Nonlinear propagation of fs laser pulses in liquids and evolution of supercontinuum generation," Opt. Express **13**(25), 10248–10259 (2005).
11. L. Guyon, K. Hajek, F. Courvoisier, *et al.*, "Control of lasing filament arrays in nonlinear liquid media," Appl. Phys. B **90**(3-4), 383–390 (2008).
12. D. P. Shelton, "Nonlocal hyper-rayleigh scattering from liquid nitrobenzene," The J. Chem. Phys. **132**(15), 154506 (2010).
13. D. Psaltis, S. R. Quake, and C. Yang, "Developing optofluidic technology through the fusion of microfluidics and optics," Nature **442**(7101), 381–386 (2006).
14. C. Monat, P. Domachuk, and B. Eggleton, "Integrated optofluidics: A new river of light," Nat. Photonics **1**(2), 106–114 (2007).
15. K. Kuhler, E. L. Dereniak, and M. Buchanan, "Measurement of the index of refraction of the plastic Phenoxy PKFE," Appl. Opt. **30**(13), 1711–1714 (1991).
16. S. Kedenburg, M. Vieweg, T. Gissibl, *et al.*, "Linear refractive index and absorption measurements of nonlinear optical liquids in the visible and near-infrared spectral region," Opt. Mater. Express **2**(11), 1588–1611 (2012).
17. J. E. Saunders, C. Sanders, H. Chen, *et al.*, "Refractive indices of common solvents and solutions at 1550 nm," Appl. Opt. **55**(4), 947–953 (2016).
18. B. Chandra and S. Bhaiya, "A simple, accurate alternative to the minimum deviation method of determining the refractive index of liquids," Am. J. Phys. **51**(2), 160–161 (1983).
19. D. Jenkins, "Refractive indices of solutions," Phys. Educ. **17**(2), 82–83 (1982).
20. A. Zaidi, Y. Makdisi, K. Bhatia, *et al.*, "Accurate method for the determination of the refractive index of liquids using a laser," Rev. Sci. Instrum. **60**(4), 803–805 (1989).
21. H. Hattori, H. Yamanaka, H. Kurniawan, *et al.*, "Using minimum deviation of a secondary rainbow and its application to water analysis in a high-precision, refractive-index comparator for liquids," Appl. Opt. **36**(22), 5552–5556 (1997).
22. H. Hattori, H. Kakui, H. Kurniawan, *et al.*, "Liquid refractometry by the rainbow method," Appl. Opt. **37**(19), 4123–4129 (1998).
23. S. Nemoto, "Measurement of the refractive index of liquid using laser beam displacement," Appl. Opt. **31**(31), 6690–6694 (1992).
24. F. Docchio, S. Corini, M. Perini, *et al.*, "A simple and reliable system for measuring the refractive index of liquids using a position-sensitive detector," IEEE Trans. Instrum. Meas. **44**(1), 68–70 (1995).
25. D. P. Shelton, "Refractive index measured by laser beam displacement at λ= 1064 nm for solvents and deuterated solvents," Appl. Opt. **50**(21), 4091–4098 (2011).
26. X. Wu, M. Muntzeck, T. de Los Arcos, *et al.*, "Determination of the refractive indices of ionic liquids by ellipsometry, and their application as immersion liquids," Appl. Opt. **57**(31), 9215–9222 (2018).
27. X. Li, C. Wang, L. Ma, *et al.*, "Ellipsometry-transmission measurement of the complex refractive indices for a series of organic solvents in the 200–1700 nm spectral range," Infrared Phys. & Technol. **125**, 104313 (2022).
28. T. L. Myers, R. G. Tonkyn, T. O. Danby, *et al.*, "Accurate measurement of the optical constants n and k for a series of 57 inorganic and organic liquids for optical modeling and detection," Appl. Spectrosc. **72**(4), 535–550 (2018).
29. C. Gouveia, M. Zibaii, H. Latifi, *et al.*, "High resolution temperature independent refractive index measurement using differential white light interferometry," Sensors Actuators B: Chem. **188**, 1212–1217 (2013).
30. C. Sainz, J. Calatroni, and G. Tribillon, "Refractometry of liquid samples with spectrally resolved white light interferometry," Meas. Sci. Technol. **1**(4), 356–361 (1990).
31. A. Guerrero, C. Sainz, H. Perrin, *et al.*, "Refractive index distribution measurements by means of spectrally-resolved white-light interferometry," Opt. & Laser Technol. **24**(6), 333–339 (1992).
32. S. Singh, "Refractive index measurement and its applications," Phys. Scr. **65**(2), 167–180 (2002).
33. H. El-Kashef, "The necessary requirements imposed on polar dielectric laser dye solvents," Phys. B **279**(4), 295–301 (2000).
34. H. El-Kashef, "Study of the refractive properties of laser dye solvents: toluene, carbon disulphide, chloroform, and benzene," Opt. Mater. **20**(2), 81–86 (2002).
35. S. De Nicola, P. Ferraro, A. Finizio, *et al.*, "Reflective grating interferometer for measuring the refractive index of transparent materials," Opt. Commun. **118**(5-6), 491–494 (1995).
36. P. Marteau, G. Montixi, J. Obriot, *et al.*, "An accurate method for the refractive index measurements of liquids: Application of the kramers–kronig relation in the liquid phase," Rev. Sci. Instrum. **62**(1), 42–46 (1991).
37. P. Hariharan, *Optical Interferometry* (Academic Press, 1985).
38. H. J. Chang, N. Munera, C. Lopez-Zelaya, *et al.*, "Refractive index and transmittance measurements of liquids from the visible to SWIR," figshare, 2024, https://doi.org/10.6084/m9.figshare.25506463.
39. K. Moutzouris, M. Papamichael, S. C. Betsis, *et al.*, "Refractive, dispersive and thermo-optic properties of twelve organic solvents in the visible and near-infrared," Appl. Phys. B **116**(3), 617–622 (2014).
40. A. Samoc, M. Samoc, B. Luther-Davies, *et al.*, "Third-order optical nonlinearities of poly (arylamino-phenylenevinylene) studied with femtosecond pulses," in *Optoelectronics, Materials, and Devices for Communications*, vol. 4580 (SPIE, 2001), pp. 347–356.
41. I. Z. Kozma, P. Krok, and E. Riedle, "Direct measurement of the group-velocity mismatch and derivation of the refractive-index dispersion for a variety of solvents in the ultraviolet," J. Opt. Soc. Am. B **22**(7), 1479–1485 (2005).

Optical Materials EXPRESS

42. J. E. Bertie, Z. Lan, R. N. Jones, *et al.*, "Infrared intensities of liquids XVIII: Accurate optical constants and molar absorption coefficients between 6500 and 800 cm- 1 of dichloromethane at 25° c, from spectra recorded in several laboratories," Appl. Spectrosc. **49**(6), 840–851 (1995).
43. S. Ghosal, J. L. Ebert, and S. A. Self, "The infrared refractive indices of CHBr3, CCl4 and CS2," Infrared Phys. **34**(6), 621–628 (1993).
44. J. N. Hayes, "Thermal blooming of laser beams in fluids," Appl. Opt. **11**(2), 455–461 (1972).
45. P. Linstorm, "NIST Chemistry webbook, NIST standard reference database number 69," J. Phys. Chem. Ref. Data, Monograph **9**, 1–1951 (1998).
46. "AIST: Spectral database for organic compounds, SDBS," https://sdbs.db.aist.go.jp/sdbs/cgi-bin/direct_frame_top.cgi. Accessed: 2023-05-25.
47. C. Wohlfarth and M. Lechner, *Refractive Indices of Pure Liquids and Binary Liquid Mixtures (Supplement to III/38)*, Landolt-Börnstein: Numerical Data and Functional Relationships in Science and Technology - New Series (Springer Berlin Heidelberg, 2008).